Journal of Alloys and Compounds 509 (2011) 4290–4294

Contents lists available at ScienceDirect

Journal of Alloys and Compounds

journal homepage: www.elsevier.com/locate/jallcom

Structural, dielectric and magnetic properties of Nd-doped Co_2Z-type hexaferrites

Jijing Xu [a], Guijuan Ji [a], Haifeng Zou [a], Yuan Zhou [b], Shucai Gan [a,*]

[a] College of Chemistry, Jilin University, Changchun 130026, China
[b] Division of Chemistry and Biological Chemistry, School of Physical and Mathematical Sciences, Nanyang Technological University, Singapore 637616, Singapore

ARTICLE INFO

Article history:
Received 6 August 2010
Received in revised form 3 January 2011
Accepted 4 January 2011
Available online 12 January 2011

Keywords:
Ferrites
Microstructure
Dielectric properties
Magnetic properties

ABSTRACT

Z-type hexaferrites doped with Nd^{3+}, $Ba_{3-x}Nd_xCo_2Fe_{24}O_{41}$ ($x = 0, 0.05, 0.10, 0.15$, and 0.25), were prepared by solid-state reaction. The effect of the Nd^{3+} ions substitution for Ba^{2+} ions on the microstructure and electromagnetic properties of the samples was investigated. The results reveal that an important modification of microstructure, complex permeability, complex permittivity, and static magnetic properties can be obtained by introducing a relatively small amount of Nd^{3+} instead of Ba^{2+}. SEM image shows that the grains of the ferrites doped with Nd^{3+} were smaller, more perfect and homogeneous than that of the pure ferrite. The real part (ε') of complex permittivity and imaginary part (ε'') increase at first, and then decrease with increasing Nd content. At low frequency, the imaginary part μ'' of complex permeability decreases with Nd content and then increases when frequency is above 7.0 GHz. The magnetization (M_s) and the coercivity (H_c) are 79.38 emu g^{-1} and 36.94 Oe for $Ba_{2.75}Nd_{0.25}Co_2Fe_{24}O_{41}$. The data of magnetism show that the ferrite doped with Nd^{3+} ions is a better soft magnetic material due to the higher magnetization and lower coercivity.

1. Introduction

Z-type hexaferrite $Ba_3Co_2Fe_{24}O_{41}$ has recently attracted great attention because of its high ferromagnetic resonance frequency, and high permeability and high thermal stability in the GHz region [1]. This material is one of the most widely used soft materials, instead of spinel ferrite, for high-frequency application, such as chip inductors, LC filters and megahertz–gigahertz (MHz–GHz) antenna [2]. From the crystallographic point of view, Z-type ferrite is among the most complex compounds in the families of hexaferrites with planar hexagonal structure [3]. This structure may be described as a stack of six kinds of blocks, R, S, T, R*, S* and T*, where R, S, and T are independent and the asterisk indicates the same stack but rotated 180° around the *c*-axis. The stacking order is RSTSR*S*T*S* [4]. Z-type hexaferrite can be treated as a sum of two simple hexaferrites, namely, M-($BaFe_{12}O_{19}$) and Y-($Ba_2Me_2Fe_{12}O_{22}$) types [3]. The dielectric and magnetic properties of hexaferrites such as, permittivity, permeability, coercivity and saturation magnetization can be controlled by substitution of divalent or trivalent ions. It is reported that ions substitution may improve their properties and characteristics [5–10]. Rare-earth elements (R) have typical relaxation characteristics, which can affect the electromagnetic properties of ferrite strongly [11–15]. Latest breakthrough is based on the partial substitution of rare-earth elements at Ba and Fe site, as $Ba_3(Co_{0.4}Zn_{0.6})_2Y_xFe_{24-x}O_{41}$ [16], $3(Ba_{0.5}Sr_{0.5})\cdot 2CoO\cdot 0.05Tb_4O_7\cdot 10.8Fe_2O_3$ and $3(Ba_{0.5}Sr_{0.5})\cdot 2CoO\cdot 0.05Gd_2O_3\cdot 10.8Fe_2O_3$ [17]. However, the microstructure and electromagnetic properties of $Ba_{3-x}Nd_xCo_2Fe_{24}O_{41}$ have not been given much attention.

We seek to provide valuable information about structural, dielectric and magnetic properties of Nd-substituted Co_2Z-type hexaferrites. In the present work, the $Ba_{3-x}Nd_xCo_2Fe_{24}O_{41}$ ($x = 0$, 0.05, 0.10, 0.15, and 0.25) ferrites were synthesized and the effect of the substitution of Nd^{3+} for Ba^{2+} on the microstructures and electromagnetic properties of the hexaferrites was investigated. In addition, the relationship between electromagnetic properties and microstructure for $Ba_{3-x}Co_2Nd_xFe_{24}O_{41}$ was investigated.

2. Experimental details

$Ba_{3-x}Nd_xCo_2Fe_{24}O_{41}$ ($x = 0$, 0.05, 0.10, 0.15, and 0.25) were prepared by the conventional ceramic process. The starting materials, Fe_2O_3, Co_2O_3, $BaCO_3$ and Nd_2O_3 were stoichiometrically weighed and milled in an agate mortar for 5 h. Then the mixed powders were calcined at 1250 °C for 5 h in air.

The crystalline phases were characterized by X-ray diffraction (XRD, BRUKER D8, Germany). These data were recorded using Cu Kα radiation at 40.0 kV and 40.0 mA in the region of $2\theta = 10$–80° with a scanning speed of 2°/min. The particle morphology was examined by field emission scanning electron microscopy (FE-SEM, FEI XL30, USA). The magnetic properties were measured by vibrating sample magnetometer (VSM, VSM7300, USA). The frequency dependence of permeability and permittivity was measured by vector network analysis measurement (VNA, Agilent PNA 8363B, USA). The magnitude of external magnetic field applied is −9750–9750 Oe. The samples were prepared as follows: the ferrite–paraffin wax compositions with 75 wt% of ferrite prepared by homogeneously mixing the ferrite powder and toroidal-shaped samples of 3.04 mm inner diameter, 7.00 mm outer diameter and 3.00–3.50 mm length. ε', ε'', μ' and μ'' were detected at the frequency range of 0–18 GHz.

* Corresponding author. Tel.: +86 431 88502259.
E-mail address: gansc@jlu.edu.cn (S. Gan).

0925-8388/$ – see front matter © 2011 Elsevier B.V. All rights reserved.
doi:10.1016/j.jallcom.2011.01.027

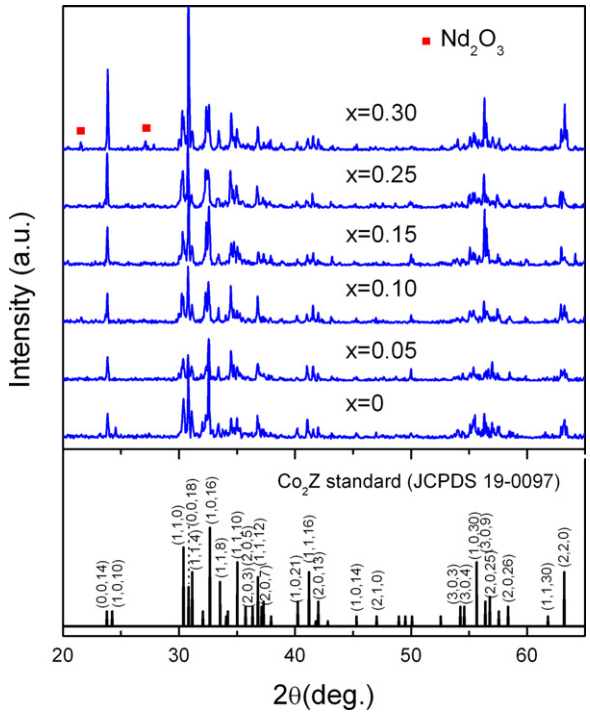

Fig. 1. XRD patterns of $Ba_{3-x}Nd_xCo_2Fe_{24}O_{41}$ as a function of x at 1250 °C for 5 h.

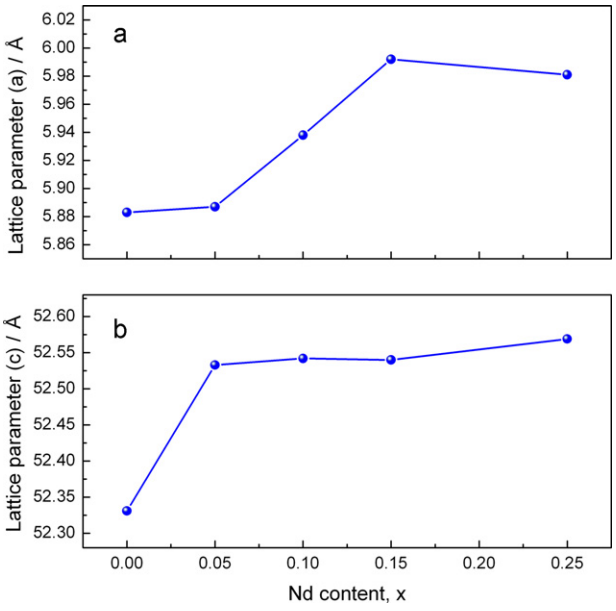

Fig. 2. The variation of lattice parameter (a and c) as a function of x.

3. Results and discussion

3.1. Structure and microstructure

X-ray diffraction patterns of the sintered samples with $x = 0$, 0.05, 0.10, 0.15, 0.25, and 0.30 are shown in Fig. 1. It can be seen that all the samples are mainly Z-type phase when $x \leq 0.25$. When $x > 0.25$, the position of the strongest peaks changed and Nd_2O_3 phase appeared. It is shown that the maximum substitution content of Ba^{2+} by Nd^{3+} is 0.25 under our experimental condition. The lattice constants (a, c and a/c), cell volume (V_{cell}), X-ray density (ρ_x), bulk density (ρ_m) and the porosity (P) are calculated by the following equations [18]:

$$d_{hkl} = \frac{1}{\sqrt{4(h^2 + hk + k^2)/3a^2 + l^2/c^2}} \quad (1)$$

$$V_{cell} = \frac{\sqrt{3}}{2} a^2 c \quad (2)$$

$$\rho_x = \frac{ZM}{N_A V_{cell}} \quad (3)$$

$$\rho_m = \frac{m}{\pi r^2 h} \quad (4)$$

$$P = 1 - \frac{\rho_m}{\rho_x} \quad (5)$$

where d_{hkl} is the d-spacing values of the lines in the XRD pattern and h, k and l are the corresponding Miller indices. M is the molar mass, m is mass of pellet, r is radius of the pellet, N_A is Avogadro's number, Z is the number of molecules per unit cell ($Z = 2$ for Z-type hexaferrite). As shown in Table 1, the calculated values of the lattice parameters a (5.883–5.992 Å), c (52.331–52.569 Å) and cell volume (1568.46–1633.62 Å^3) are closer to the reported literature values [3]. Variation of lattice parameters (a, c) as a function of Nd content is shown in Fig. 2. It is evident that the a, c and the ratio of c/a increase with increasing Nd content. This is expected because the charge density of Nd^{3+} is stronger than that of the Ba^{2+}, the repulsions of Nd^{3+} with the surrounding ions in the lattice would be increased. In order to minimize the repulsion and maintain overall stability of the structure, the crystal structure expands and that leads to the increasing of the values a and c. This suggests that the substitution ions, which have been placed on the crystal sites of barium ferrite, affect the electromagnetic properties of this material. Fig. 3 shows the variation of the bulk density (ρ_m), X-ray density (ρ_x) and the porosity (P) as a function of Nd content x. With increasing Nd content, the bulk density decreases and the porosity increases slightly. This behavior may be attributed to the fact that the introduction of Nd ions in hexaferrite affects the grain size development during sintering. The elemental compositions of the synthesized $Ba_{3-x}Nd_xCo_2Fe_{24}O_{41}$ ($x = 0.00$–0.25) were

Table 1
Lattice constants (a, c and a/c), cell volume (V_{cell}), X-ray density (ρ_x), bulk density (ρ_m), porosity (P), magnetization (M_s), coercivity (H_c) and elemental compositions of $Ba_{3-x}Nd_xCo_2Fe_{24}O_{41}$.

Parameters	Nd content, x				
	$x = 0$	$x = 0.05$	$x = 0.10$	$x = 0.15$	$x = 0.25$
Lattice constant, a (Å)	5.883	5.887	5.938	5.992	5.981
Lattice constant, c (Å)	52.331	52.533	52.542	52.540	52.569
Aspect ratio, a/c	0.1124	0.1121	0.1130	0.1140	0.1138
Cell volume, V_{cell} (Å^3)	1568.46	1576.66	1604.37	1633.62	1628.53
Bulk density, ρ_m (g cm^{-3})	4.06	3.99	3.92	3.80	3.77
X-ray density, ρ_x (g cm^{-3})	5.35	5.32	5.23	5.14	5.16
Porosity, P (%)	0.24	0.25	0.25	0.26	0.27
Magnetization, M_s (emu g^{-1})	61.36	70.00	73.82	76.24	79.38
Coercivity, H_c (Oe)	47.22	40.23	41.79	41.97	36.94

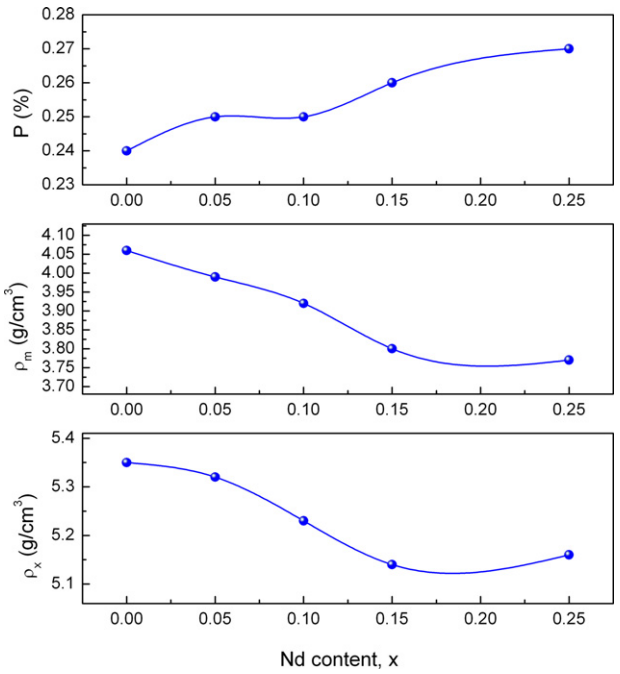

Fig. 3. Variation of X-ray density (ρ_x), bulk density (ρ_m), and porosity (P) with a variation in the Nd content x of the $Ba_{3-x}Nd_xCo_2Fe_{24}O_{41}$ (x = 0.00–0.25).

shown in Table 1. Chemical analysis data indicate that the molecular percentage ratio is in good agreement with theoretic value (Table 2).

Fig. 4 shows SEM images of $Ba_{3-x}Nd_xCo_2Fe_{24}O_{41}$ (x = 0, 0.05, 0.10, 0.15, and 0.25) samples. All the ferrites show well crystalline nature with an almost uniform grain size distribution. The grain size of the pure sample (average grain size: about 15 μm) appears to be bigger than that of the doped samples (average grain size: 5–10 μm). This is probably caused by the Nd^{3+} doping which could inhibit the development of grain size. This result agrees well with

Table 2
Elemental compositions of $Ba_{3-x}Nd_xCo_2Fe_{24}O_{41}$.

Parameters	Nd content, x				
	x = 0	x = 0.05	x = 0.10	x = 0.15	x = 0.25
Ratio, Ba/mol	3.07	2.95	2.86	2.84	2.76
Ratio, Fe/mol	24.40	24.12	24.20	24.22	24.36
Ratio, Co/mol	2.00	2.00	2.00	2.00	2.00
Ratio, Nd/mol	0	0.05	0.11	0.14	0.26

X-ray data, where the values of the lattice parameters increase gradually with increasing Nd content, which leads to the crystalline deformation and inner stress.

3.2. Permittivity and permeability

In order to estimate the dielectric and dynamic magnetic properties of the samples, the complex permittivity ($\varepsilon_r = \varepsilon' + j\varepsilon''$) and complex permeability ($\mu_r = \mu' + j\mu''$) were studied. The frequency dependence of ε', ε'', μ', and μ'' for Nd substituted barium ferrites with different Nd content are shown in Figs. 5 and 6.

Fig. 5(a and b) shows frequency spectra of complex permittivity of the $Ba_{3-x}Nd_xCo_2Fe_{24}O_{41}$ samples over frequency range 0–18.0 GHz. It is obvious that the ε' and ε'' increase firstly with Nd doping when x < 0.15 and then decrease sharply at higher doping content. In general, the dielectric properties of polycrystalline ferrite arise mainly due to the interfacial polarization and intrinsic electric dipole polarization [19]. The substitution of Nd^{3+} for Ba^{2+} leads to a change in Fe^{3+} ions to Fe^{2+} in order to balance the electrical valence, and this replacement contribute to the increment of interfacial polarization with the increase of Fe^{2+} ions because Fe^{2+} ions are easily polarized. On the other hand, the mechanism of intrinsic electric dipole polarization is due to electronic transfer between Fe^{2+} and Fe^{3+} on the octahedral sites [20]. With the increase of Fe^{2+}, the chance of electron hopping increases, this could lead to higher permittivity. However, permittivity decreases for x = 0.15 and 0.25, due to the variation of microstructure (porosity, grain boundary, etc.). In the samples with less density, more poros-

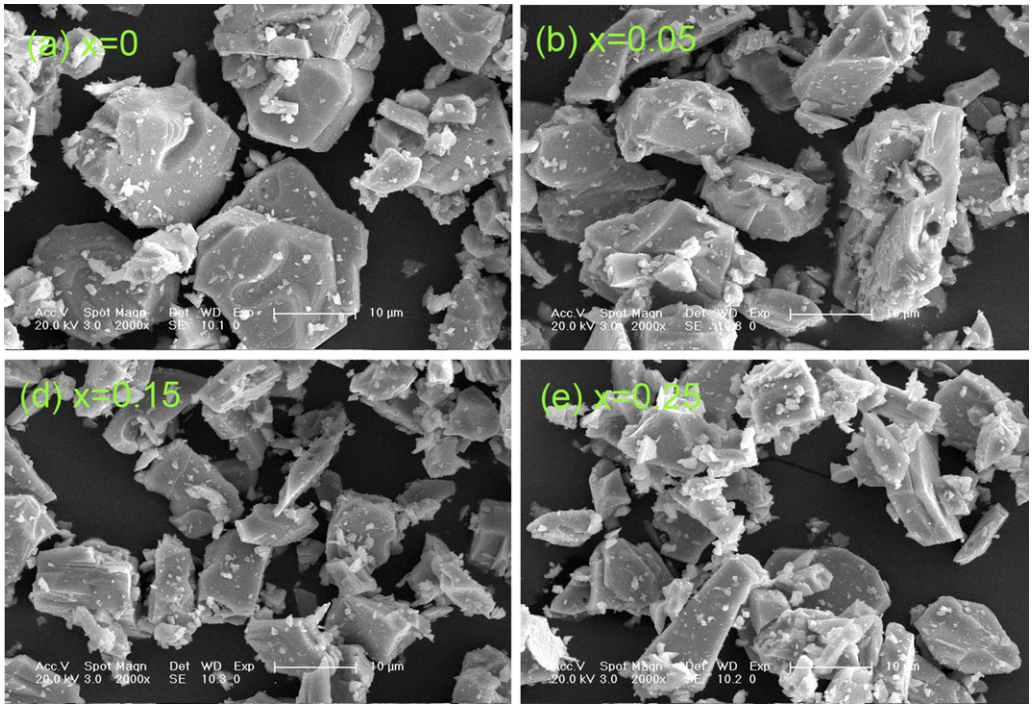

Fig. 4. SEM micrographs of the samples in series $Ba_{3-x}Nd_xCo_2Fe_{24}O_{41}$ (x = 0.00–0.25).

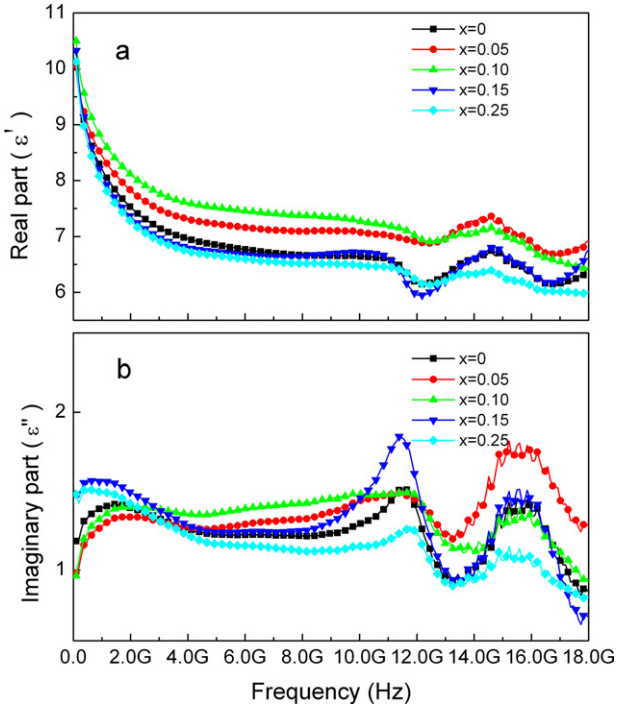

Fig. 5. Frequency dependence of complex permittivity (ε' and ε'') of the $Ba_{3-x}Nd_xCo_2Fe_{24}O_{41}$ ($x = 0.00$–0.25).

ity and grain boundary will reduce the permittivity dramatically [21]. The porosity and grain boundary increase with the increasing Nd content as shown in Figs. 1 and 4.

The frequency spectra of complex permeability of the $Ba_{3-x}Nd_xCo_2Fe_{24}O_{41}$ samples over frequency range 0–18.0 GHz is shown in Fig. 6(a and b). In Fig. 6(a), the values of the μ' decrease monotonously with frequency, which can be ascribed to relaxation phenomena of domain magnetization rotation or domain wall dis-

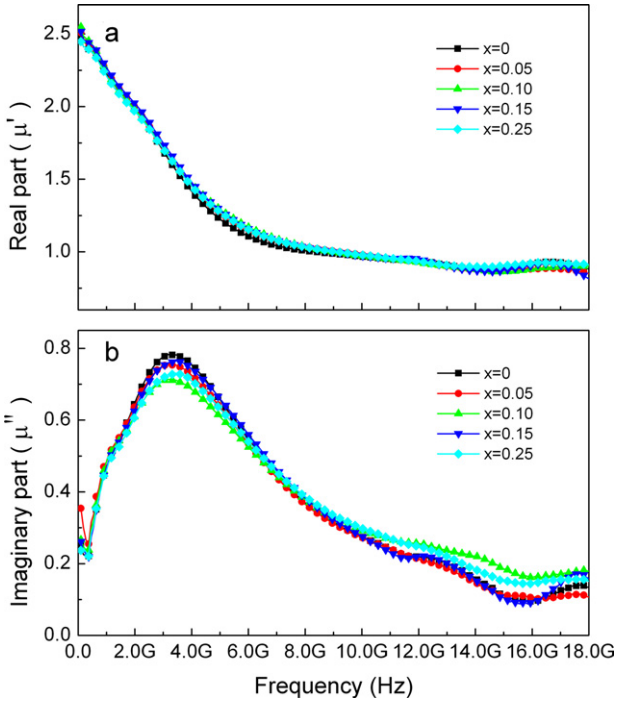

Fig. 6. Frequency dependence of complex permeability (μ' and μ'') of the $Ba_{3-x}Nd_xCo_2Fe_{24}O_{41}$ ($x = 0.00$–0.25).

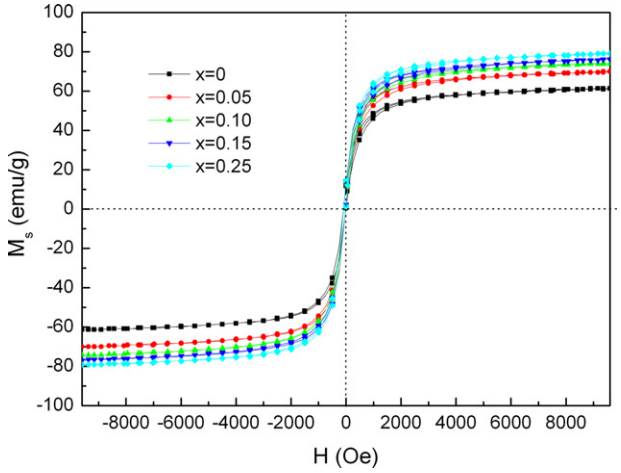

Fig. 7. Hysteresis loops of the $Ba_{3-x}Nd_xCo_2Fe_{24}O_{41}$ ($x = 0.00$–0.25).

placement occurring in the GHz region [22]. There is no obvious change of μ' for different Nd contents. It can be seen in Fig. 6(b) that each ferrite has a peak value in the imaginary part μ''. The peak value of μ'' is caused by natural resonance and domain wall resonance phenomena. According to electromagnetic theory, the μ'' is influenced by M_s and H_A according to the equation [10],

$$\mu'' = \frac{M_s}{2H_A\alpha} \tag{6}$$

where M_s, H_A and α are saturation magnetization, magneto-crystal anisotropy field, and extinction coefficient, respectively. VSM results show that the saturation magnetization M_s almost increases with the Nd content (Table 1). In addition, the presence of Fe^{2+} at 2a site could positively contribute to the enhancement of the magneto-crystalline anisotropy H_A [23]. As shown in Fig. 6(b), it is believed that the main effect on μ'' comes from the increase of the magneto-crystal anisotropy field when frequency is less than 7.0 GHz. Therefore, μ'' decreases after Nd^{3+} is doped. At high frequency (above 7.0 GHz), μ'' increases when the magnetization is regarded as dominant source.

3.3. Magnetic parameters

The hysteresis loops for the $Ba_{3-x}Nd_xCo_2Fe_{24}O_{41}$ ($x = 0$–0.3) samples are shown in Fig. 7 and the values of saturation magnetization (M_s), remanence (M_r), and coercivity (H_c) are listed in Table 1. All the samples exhibit typical soft magnetic character with low coercivity. It is clear that the saturation magnetization increases with the Nd doping. As mentioned above, the substitution of Nd^{3+} for Ba^{2+} led to the change of Fe^{3+} to Fe^{2+} at 2a sites. As a result, the enhancement of the Fe^{3+}–O–Fe^{3+} super-exchange interaction increased in the hyperfine field at 12k and 2b sites, which led to the increase of M_s [24]. The coercivity H_c slightly decreases after Nd^{3+} is doped because the aspect ratio (a/c) increases as shown in Table 1. In that case the coercivity could be expressed as follows:

$$H_c = 0.48\left[\frac{K_1}{M_s} - N_d M_s\right] \tag{7}$$

where C is a constant, K_1 is the magneto-crystalline anisotropy constant, M_s is the saturation magnetization and N_d is the demagnetizing coefficient relating to the shape anisotropy. The aspect ratio could enhance the demagnetizing factor and thus reduce H_c [25].

4. Conclusions

Minor Nd doping ($x = 0.05$–0.25) will not destroy the phase formation of Z-type hexaferrite. Nd doping suppressed the grain growth and decreased the grain size. The novel Nd-doped Z-type ferrites exhibit excellent static magnetic properties such as high saturation magnetization up to 79.38 emu g^{-1} and low coercivity under 40 Oe. With increasing Nd content, the ε' and ε'' increase at first, and then decrease. At low frequency (below 7.0 GHz), the imaginary part μ'' of complex permeability decreases with Nd content and then increases when frequency is above 7.0 GHz. Domain wall resonance and natural resonance phenomena are observed in μ'' spectra for all the samples.

Acknowledgements

This work was supported by the Hi-Tech Research and Development Program of China (Grant no. 2007AA06Z202) and the National Science and Technology Major Projects (Grant no. 2008ZX05018).

References

[1] S. Bae, Y.K. Hong, J.J. Lee, J. Jalli, G.S. Abo, A. Lyle, I.T. Nam, W.M. Seong, J.S. Kum, S.H. Park, IEEE Trans. Magn. 45 (2009) 2557–2560.
[2] X.H. Wang, L.T. Li, S.Y. Su, Z.L. Gui, J. Am. Ceram. Soc. 88 (2005) 478–480.
[3] J.J. Xu, C.M. Yang, H.F. Zou, Y.H. Song, G.M. Gao, B.C. An, S.C. Gan, J. Magn. Magn. Mater. 321 (2009) 3231–3235.
[4] L. Jia, Y. Tang, H. Zhang, P. Deng, Y. Liu, B. Liu, Jpn. J. Appl. Phys. 49 (2010) 063001.
[5] G.F.M. Pires Júnior, H.O. Rodrigues, J.S. Almeida, E.O. Sancho, J.C. Góes, M.M. Costa, J.C. Denardin, A.S.B. Sombra, J. Alloys Compd. 493 (2010) 326–334.
[6] M.J. Iqbal, M.N. Ashiq, P. Hernández-Gómez, J.M.M. Muñoz, C.T. Cabrera, J. Alloys Compd. 500 (2010) 113–116.
[7] Z.F. Zi, H.Y. Liu, Y.N. Liu, L. Fang, Q.C. Liu, J.M. Dai, X.B. Zhu, Y.P. Sun, J. Magn. Magn. Mater. 332 (2010) 3638–3641.
[8] Z. Chen, A. Yang, K. Mahalingam, K.L. Averett, J. Gao, G.J. Brown, C. Vittoria, V.G. Harris, Appl. Phys. Lett. 96 (2010) 242502.
[9] Y.J. Kim, S.S. Kim, J. Electroceram. 24 (2010) 314–318.
[10] L.X. Wang, J. Song, Q.T. Zhang, X.G. Huang, N.C. Xu, J. Alloys Compd. 481 (2009) 863–866.
[11] G.M. Rai, M.A. Iqbal, K.T. Kubra, J. Alloys Compd. 495 (2010) 229–233.
[12] Y. Liu, M.G.B. Drew, Y. Liu, J.P. Wang, M.L. Zhang, J. Magn. Magn. Mater. 332 (2010) 3342–3345.
[13] M.J. Iqbal, S. Farooq, J. Alloys Compd. 505 (2010) 560–567.
[14] Z.Y. Pang, X.J. Zhang, B.M. Ding, D.X. Bao, B.S. Han, J. Alloys Compd. 492 (2010) 691–694.
[15] R.S. Meena, S. Bhattachrya, R. Chatterjee, J. Magn. Magn. Mater. 332 (2010) 1923–1928.
[16] L.J. Jia, J. Luo, H.W. Zhang, Y.L. Jing, Y. Shi, J. Magn. Magn. Mater. 321 (2009) 77–80.
[17] S.H. Guo, Y.H. Zhang, Z.K. Feng, X.L. Wang, H.H. He, J. Rare Earth 25 (2007) 220–222.
[18] M.J. Iqbal, M.N. Ashiq, Chem. Eng. J. 136 (2008) 383–389.
[19] A.K. Singh, T.C. Goel, R.G. Mendiratta, O.P. Thakur, C. Prakash, J. Appl. Phys. 91 (2002) 6626–6629.
[20] G.Z. Shen, Z. Xu, Y. Li, J. Magn. Magn. Mater. 301 (2006) 325–330.
[21] Y. Bai, J. Zhou, Z.L. Gui, L.T. Li, L.J. Qiao, J. Alloys Compd. 450 (2008) 412–416.
[22] S.E. Jacobo, W.G. Fano, A.C. Razzitte, N.D. Digiovanni, V. Trainotti, El. Insulation and Diel. Phenomena, Annual Report Conference, vol. 1, 1998, pp. 273–276.
[23] S. Ounnunkad, Solid State Commun. 138 (2006) 472–475.
[24] Y. Han, J. Sha, L. Sun, Q. Tang, Q. Lu, H. Jin, D. Jin, H. Bo, H. Ge, X. Wang, J. Alloys Compd. 486 (2009) 348–351.
[25] X.S. Liu, W. Zhong, S. Yang, Z. Yu, B.X. Gu, Y.W. Du, J. Magn. Magn. Mater. 238 (2002) 207–214.